

Acoustofluidic Relay: Sequential Trapping and Transporting of Microparticles via Acoustically Excited Oscillating Bubbles

Yuliang Xie, Daniel Ahmed, Michael Ian Lapsley, Mengqian Lu, Sixing Li and Tony Jun Huang
Journal of Laboratory Automation 2014 19: 137 originally published online 16 April 2013
DOI: 10.1177/2211068213485748

The online version of this article can be found at:
<http://jla.sagepub.com/content/19/2/137>

Published by:



<http://www.sagepublications.com>

On behalf of:



Come Transform Research™

[Society for Laboratory Automation and Screening](http://www.slas.org)

Additional services and information for *Journal of Laboratory Automation* can be found at:

Email Alerts: <http://jla.sagepub.com/cgi/alerts>

Subscriptions: <http://jla.sagepub.com/subscriptions>

Reprints: <http://www.sagepub.com/journalsReprints.nav>


Permissions: <http://www.sagepub.com/journalsPermissions.nav>

>> [Version of Record](#) - Mar 17, 2014

[OnlineFirst Version of Record](#) - Apr 16, 2013

[What is This?](#)

Acoustofluidic Relay: Sequential Trapping and Transporting of Microparticles via Acoustically Excited Oscillating Bubbles

Journal of Laboratory Automation
2014, Vol. 19(2) 137–143
© 2013 Society for Laboratory
Automation and Screening
DOI: 10.1177/2211068213485748
jala.sagepub.com


Yuliang Xie^{1,2}, Daniel Ahmed², Michael Ian Lapsley², Mengqian Lu², Sixing Li³, and Tony Jun Huang^{1,2}

Abstract

We report an on-chip acoustofluidic method for sequential trapping and transporting of microparticles via acoustically oscillating bubbles. The size and location of bubbles were precisely controlled by lithography. When the acoustic waves were turned off, particles followed the streamlines dictated by laminar flow. When the acoustic waves were turned on, particles were attracted to and trapped in a vortex near the surface of bubble. Therefore, particles could move across the microfluidic channel with programmed trajectories. Additionally, a theoretical model based on acoustic radiation force and drag force due to acoustic microstreaming was established to help design this particle-trapping and -transporting system.

Keywords

acoustofluidics, microbubble, particle transfer, radiation force

In the past two decades, the field of microfluidics has shown great promise and affected many areas such as chemical synthesis and medical diagnostics.^{1–4} In many microfluidic-based studies and applications, such as cell separation and sorting,^{5–8} it is essential to have techniques that can actively control and manipulate the trajectories of microparticles, such as cells.⁹ To control the trajectories of microparticles, an external force field needs to be exerted on particles within a microfluidic device so that selected particles can overcome the effects of laminar flow and change their trajectories.¹⁰ Based on this principle, several methods have been successfully developed to manipulate particle trajectories. Hydrodynamic effects^{11–16} can direct particles by manipulating the laminar streamlines in certain-shaped microfluidic channels. Charged or magnetic particles can be controlled by external electric^{17–19} or magnetic fields.^{20,21} Particles can also be manipulated by optical forces using optical tweezers²² or optoelectronic tweezers.²³

Recently, acoustic methods have attracted significant attention as an alternative way to manipulate particles.²⁴ Compared with other particle manipulation approaches, acoustic manipulation offers many advantages: it is compact, noninvasive, contact free, and versatile. However, the wavelengths for most commonly used acoustic transducers are much longer than the micrometer scale, which seems unfavorable for on-chip particle manipulation. One approach to overcome this barrier is to use high-frequency (~10 MHz) acoustic transducers to achieve acoustic waves with short wavelengths (e.g., 100 μm).^{25–32} An alternative approach for acoustic manipulation is to use

acoustically oscillating bubble-based systems,^{33–48} in which the experimental setups could be significantly simplified while keeping all advantages of the previously recognized acoustic manipulation methods. In such systems, low-frequency (kHz range) acoustic waves oscillate the air-liquid interface of a bubble, and this oscillation manipulates the particles through the relatively strong effects of acoustic streaming and radiation force. Even at low frequencies (kHz range), this oscillatory response is confined to a region comparable with the radius of the bubble (~100 μm), which makes it possible to achieve on-chip control of the particle trajectory. A few researchers reported the trapping and manipulation of particles using acoustically oscillating bubbles^{33,34,37,38,40,41,44–46}; however, the particle-trapping effect occurs only in short range because of the limited working range of a single oscillating bubble. In addition, in these approaches, the position and size of the bubbles were difficult to control. Therefore, to develop a practical, on-chip, particle manipulation method using acoustically

¹Department of Chemical Engineering, The Pennsylvania State University, University Park, PA, USA

²Department of Engineering Science and Mechanics, The Pennsylvania State University, University Park, PA, USA

³Cell and Developmental Biology Program, The Pennsylvania State University, University Park, PA, USA

Corresponding Author:

Tony Jun Huang, Pennsylvania State University, 212 Earth-Engineering Sciences Building, University Park, PA 16802-6812, USA
Email: junhuang@psu.edu

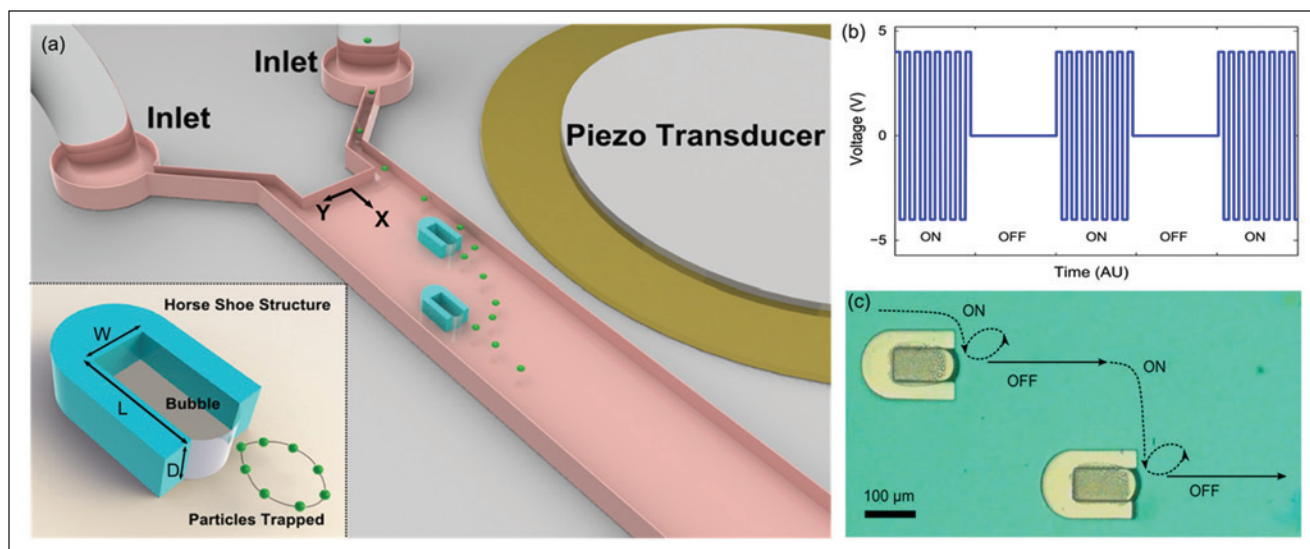


Figure 1. (a) Experimental design and setup of the acoustofluidics relay. Inset figure shows the dimensions of the horseshoe structure and particles trapped in the cycle around the bubble surface. (b) The burst mode signal to activate bubbles, with peak-to-peak voltage of 8 V and frequency of 31 kHz. (c) Image of the horseshoe structures in the microfluidic channel. The arrows indicate the typical trajectory of a particle in response to the signal in (b).

oscillating bubbles, one must use multiple bubbles with precise control on the size and location.

In this article, we report a simple, single-layer, microfluidic device that can control the trajectory of particles by acoustic oscillation of multiple bubbles trapped in horseshoe-shaped structures. Our device can conveniently and precisely control the position and size of bubbles. The bubble size determines the oscillation behavior at prescribed frequencies; the location of the bubble determines the direction to which the particles will move. Thus, we can optimize the resonance frequency of the bubbles and precisely position them to maximize particle-transporting efficiency. Moreover, by applying multiple bubbles, this device is capable of controlling the trajectories of particles in a large range, mitigating the disadvantage of using only a single bubble, whose ability to affect particle trajectory is limited to a relatively small region. The use of multiple bubbles also allows the sequential manipulation of particles, thus compounding influence on the desired trajectory and creating an acoustofluidic relay.

Materials and Methods

Device Design and Experimental Setup

The polydimethylsiloxane (PDMS)-based microchannel was fabricated using a standard soft lithography technique^{49,50} and was bonded to a glass slide (**Fig. 1a**). The channel width, depth, and length were 570 μm , 90 μm , and 1.5 cm, respectively. The device featured two horseshoe structures having widths (w), lengths (l), and depths (d) of

60, 120, and 90 μm , respectively (inset of **Fig. 1a**). The distance between the two bubbles in the x-direction was 350 μm , and the distance in the y-direction was 90 μm . When the liquid filled the channel, a bubble formed in each horseshoe structure due to surface tension. A piezoelectric transducer (model No. 273-073; Radioshack Corp., Fort Worth, TX) was bonded adjacent to the PDMS microfluidic device on the same glass substrate using epoxy (**Fig. 1a**). The piezoelectric transducer was driven by a function generator (Hewlett Packard 8116A) in a burst function mode (**Fig. 1b**). In this mode, the function generator generated a square wave during the on time (t_{ON}), with a frequency matching the natural resonant frequency of the bubbles, and no voltage was applied during the off time (t_{OFF}). The peak-to-peak voltage (V_{pp}) was set to 8 V, which generated suitable bubble oscillation amplitude to attract particles while keeping the bubble stable. The driving frequency was set at 32 kHz, which was based on the calculated resonant frequency of bubbles.

To demonstrate particle trapping and transportation, a solution of polystyrene microparticles (diameter 10 μm) in deionized (DI) water was injected through one channel inlet; the concentration of the particles was about 10^5 per milliliter. Pure DI water was supplied through the other. Without acoustic waves, the particles were confined to only one side of the channel due to laminar flow in the channel. When the piezoelectric transducer was turned on, nearby particles were attracted to the bubble and trapped in a vortex (**Fig. 1c**, dashed lines). Turning off the transducer at this time released the particles, allowing them to follow the laminar flow in the channel to the proximity of the second bubble (**Fig. 1c**, solid

lines). When the transducer was again activated for a time t_{ON} , the particles were attracted to the second bubble, after which the transducer was again deactivated and the particles were released. In this manner, an acousofluidic relay was created by alternating between the on and off states of the piezoelectric transducer. This allowed manual control of movement time across the laminar streamlines and thus manipulation of particle movement across the channel.

The particles' moving trajectories were recorded by a CCD camera (Casio Exilim Pro EX-F1) at 600 frames per second. The resulting videos were processed by Image J software to track the particle location at every frame and analyze the particle velocity.

Results

Characterization of the Resonant Frequency of Bubbles

When the piezoelectric transducer was turned on, the bubble started to oscillate, which generated fluctuations in the velocity and pressure of the liquid surrounding the bubbles and perturbed the laminar flow in the channel.⁵¹ The bubbles oscillated most effectively at their resonant frequency, which is roughly estimated by the small-amplitude behavior of the Rayleigh-Plesset equation⁵²:

$$f^2 = \frac{1}{4\rho\pi^2\alpha^2} \left[3k \left(p + \frac{2\sigma}{\alpha} \right) - \frac{2\sigma}{\alpha} \right], \quad (1)$$

where ρ is the density of the liquid (1000 kg/m³), σ is the surface tension of solution (0.0728 N/m), κ is the polytropic exponent for a bubble containing air (1.4), p is the fluidic pressure (101,325 N/m²), and α is the radius of the bubble in meters. The radius of each bubble, determined from the image in **Figure 2a**, was approximately 80 μm , and its natural resonance frequency was calculated to be 41 kHz. Experimentally, the maximum bubble oscillation was observed to be in the range of 30 to 35 kHz. The discrepancy between the experimental and calculated resonant frequencies can be attributed to the nonspherical shape of the air bubbles trapped within the horseshoe structures. **Figure 2b** shows bubble oscillation in the presence of acoustic waves. The detailed bubble oscillation behavior was characterized by a fast camera (Photron Fastcam SA4) at 225,000 fps while stimulating the bubble with 32 kHz acoustic waves. The middle point of the bubble surface was tracked (**Fig. 2c**). The experimental results verified that the bubble oscillated at about 32 kHz, almost the same as the frequency of the stimulating acoustic waves. The amplitude of the bubble oscillation was observed to be about 4.5 μm . The average oscillating velocity (u_p) of the bubble surface could be estimated by changes in bubble surface position between each frame, as 0.56 m/s.

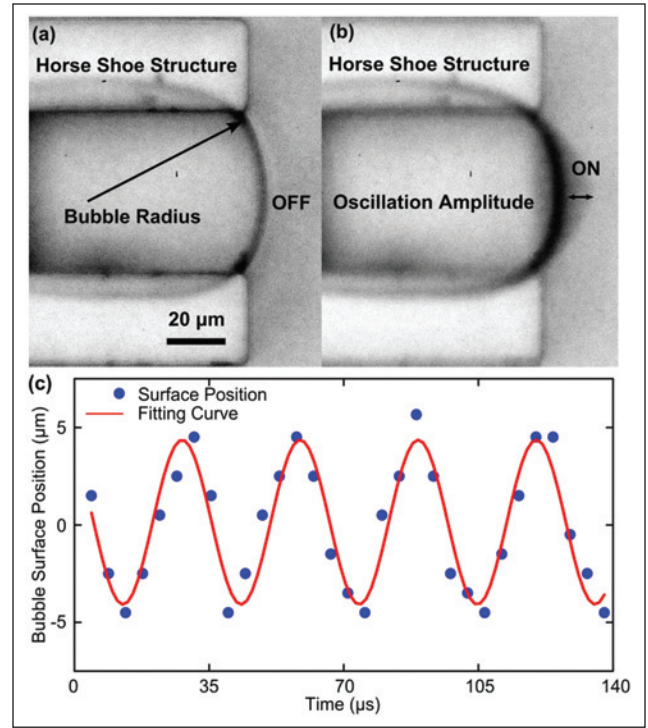


Figure 2. (a) Image of bubble with the piezoelectric transducer turned off. (b) Fast-camera image of a bubble with the piezoelectric transducer turned on, showing the amplitude of oscillation at about 4.5 μm . (c) Position of the surface of an oscillating bubble recorded from a fast camera, with the surface velocity calculated as 0.56 m/s.

Force Analysis for Particle Transport

Once microparticles were injected into the acoustic-induced fluidic field, the motion of particles was dictated by two forces: the drag force (F_d) from acoustic streaming and the acoustic radiation force (F_p). At a low Reynolds number, the drag force F_d on a spherical particle was

$$F_d = 6\pi\eta R_s v \quad (2)$$

where R_s is the radius of the particle, η is the medium viscosity, and v is the relative velocity between the particle and the fluid. However, it is very difficult to determine v at each x and y position in a flow field. Thus, we used maximum velocity (U_L) to estimate the upper limit of the velocity of a particle in the vortex. The streaming patterns generated by the oscillating bubbles were studied before⁵¹, and the maximum velocity of the liquid within the boundary layer of streaming is⁵³

$$U_L = \omega^{-1} u_0^2 R_p^4 r^{-5} \quad (3)$$

where $\omega = 2\pi f$; R_p is the radius (80 μm) of an ideal spherical acoustic source, which is approximated as the surface

curvature of the bubble in **Figure 2b**; u_0 is the velocity amplitude of the oscillating interface (calculated as 0.56 m/s by the fast camera; **Fig. 2c**), and r is the distance to the bubble surface. When the particle is introduced into the flow field, the particle Reynolds number is still very small; thus, the maximum drag force due to acoustic streaming could be estimated by

$$F_{d_{max}} = 6\pi\eta R_s U_L \quad (4)$$

The radiation force (F_r), derived by the time-averaged, second-order momentum terms in the Navier-Stokes equation,⁵⁴ also affects the particles and is described by

$$F_r = \frac{4}{3} \pi R_s^3 d_m u_0^2 B R_p^4 r^{-5} \quad (5)$$

where d is the density of the particle, d_s is the density of the medium, and $B = 3(d_s - d_m)/(2d_s + d_m)$ is the constant that determines the direction of the radiation force on the particle ($B > 0$, attractive force; $B < 0$, repulsive force). As a design parameter for our transportation system, the ratio of streaming-induced drag force and radiation force was attained by combining eqs 3, 4, and 5:

$$\frac{F_r}{F_{d_{max}}} = \frac{4}{9} \pi f d_m B R_s^2 \eta^{-1} \quad (6)$$

Equation 6 shows that with higher oscillating frequency or relatively large particle size, F_r plays a more important role in the motion of the particle than F_d , causing the particles to attract to the surface of the bubble. Otherwise, F_d would determine the trajectories of particles, and the trajectories would be similar to the streaming pattern. Because eq 6 is derived from $F_{d_{MAX}}$ rather than F_d , it provides only a qualitative analysis. Nevertheless, it is still valuable for the design of our experimental system. If the ratio in eq 6 was larger than 1, or even close to 1, F_r would dominate F_d (because F_d is always less than $F_{d_{MAX}}$) and the particles would be trapped at the surface of the bubble. On the contrary, if the ratio is much less than 1 (e.g., 0.01), the drag force would dominate the system and the particles would easily escape the vortex by following streamlines. Our design avoided these two extreme situations because the bubble radius was 80 μm , which fixed the bubble resonant frequency at 30 to 35 kHz, and the particle size was 10 μm . These parameters resulted in a balanced ratio of $F_r/F_{d_{MAX}}$ at about 0.2 to 0.3. Thus, the frequency that induced a maximum oscillation of the bubble coincided with the condition in which 10 μm particles would neither easily escape the vortex nor attach to the bubble surface. At this frequency, the particles would be trapped in the vortex near the surface of the oscillating bubble.

Particle Transport between Bubbles

The experimental results (**Fig. 3**) confirm the design principle derived from eq 6. **Figure 3a–c** shows the series of images demonstrating the transfer process of particles between the two bubbles. In **Figure 3a**, the function generator was on, which could be observed by the oscillation of the bubble. The particles were attracted to the bubble by the radiation force and trapped in a vortex near the bubble even with continuous fluid injecting from the inlet. In **Figure 3b**, the function generator was turned off, causing the particles to be released from the vortex and follow the laminar streamlines toward the outlet. The time during which the function generator was turned off was set as the time for the particles to flow from one bubble to the other along the x-direction in laminar flow. When the function generator was turned on for a second time (**Fig. 3c**), the particles moved toward the second bubble and again became trapped. When the transducer was turned off again, the particles were released and moved downstream. **Figure 3d** is a composite image displaying all of the frames of a consecutive particle transportation video. It indicates the trajectories in which all the particles follow. Dotted lines were added to indicate the trajectory of a single particle during t_{ON} and solid lines for the trajectory during t_{OFF} .

The quantitative trajectory analysis of a single particle (**Fig. 4a, b**) from our experimental results revealed additional information about the particle-trapping and -transportation process. In **Figure 4a**, before the piezoelectric transducer turned on, the particle moved almost linearly (diverging slightly due to the presence of the horseshoe structures) with constant velocity due to laminar flow in the channel. After the piezoelectric transducer was turned on (point I in **Fig. 4a**), the particle attracted to the bubble, and its velocity increased. The moving direction of the particle was not directly toward the bubble because of the injecting flow in the x-direction. The speed of the single particle during the trapping process (**Fig. 4c**) was calculated by dividing the distance between each subsequent position of the particle in the video by the time interval between each frame. When the particle was far from the bubble (point I in **Fig. 4a**), the speed was almost constant. At that distance, both the radiation force and the drag force (either from the mainstreaming or from the acoustic streaming) were too weak to significantly influence the particle motion. As the particle approached the bubble, the speed increased dramatically (point II in **Fig. 4a**). This increase in speed was caused by two factors: the fluid velocity increased due to acoustic streaming within the vortex near the bubble surface, and the radiation force increased as the particle approached the bubble. Similar analysis was applied for the rotation process in **Figure 4b and d**, in which the particle rotated in a nearly elliptical cycle. This rotation indicated that when the particle approached the surface of the bubble (point III in

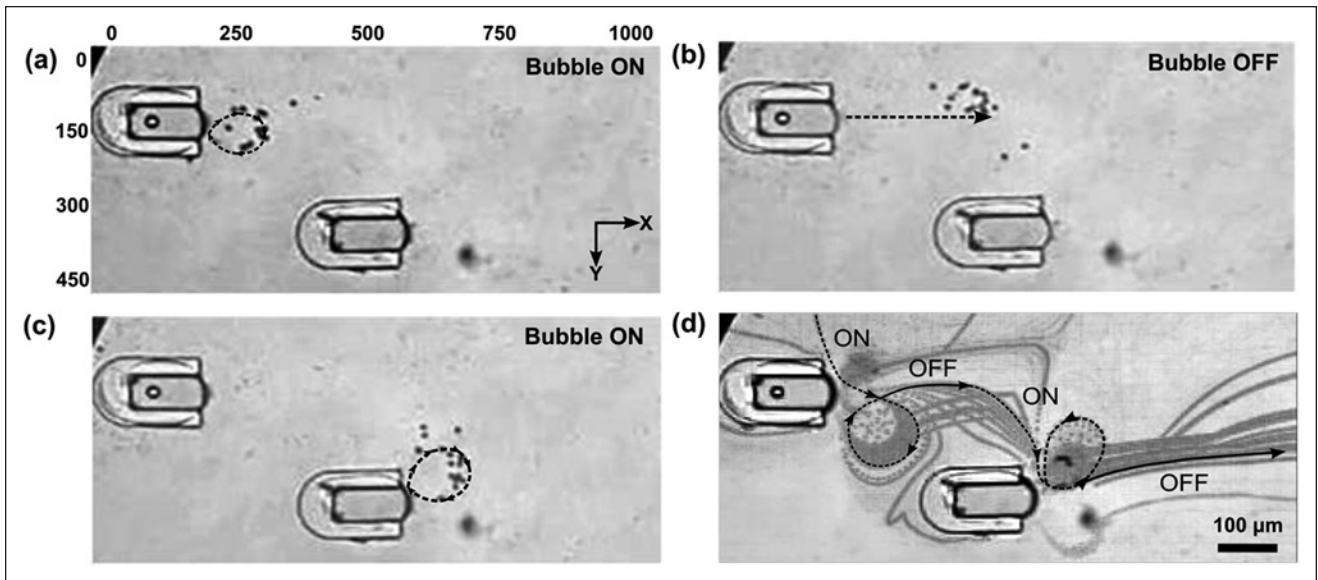


Figure 3. (a) Image of particles trapped by the first bubble. (b) Image of particles released and flowing downstream when the piezoelectric transducer was turned off. (c) Image of particles attracted and trapped to the second bubble when the piezoelectric transducer was turned on. (d) Stack of images from a video indicating the trajectories of many particles during the transportation process.

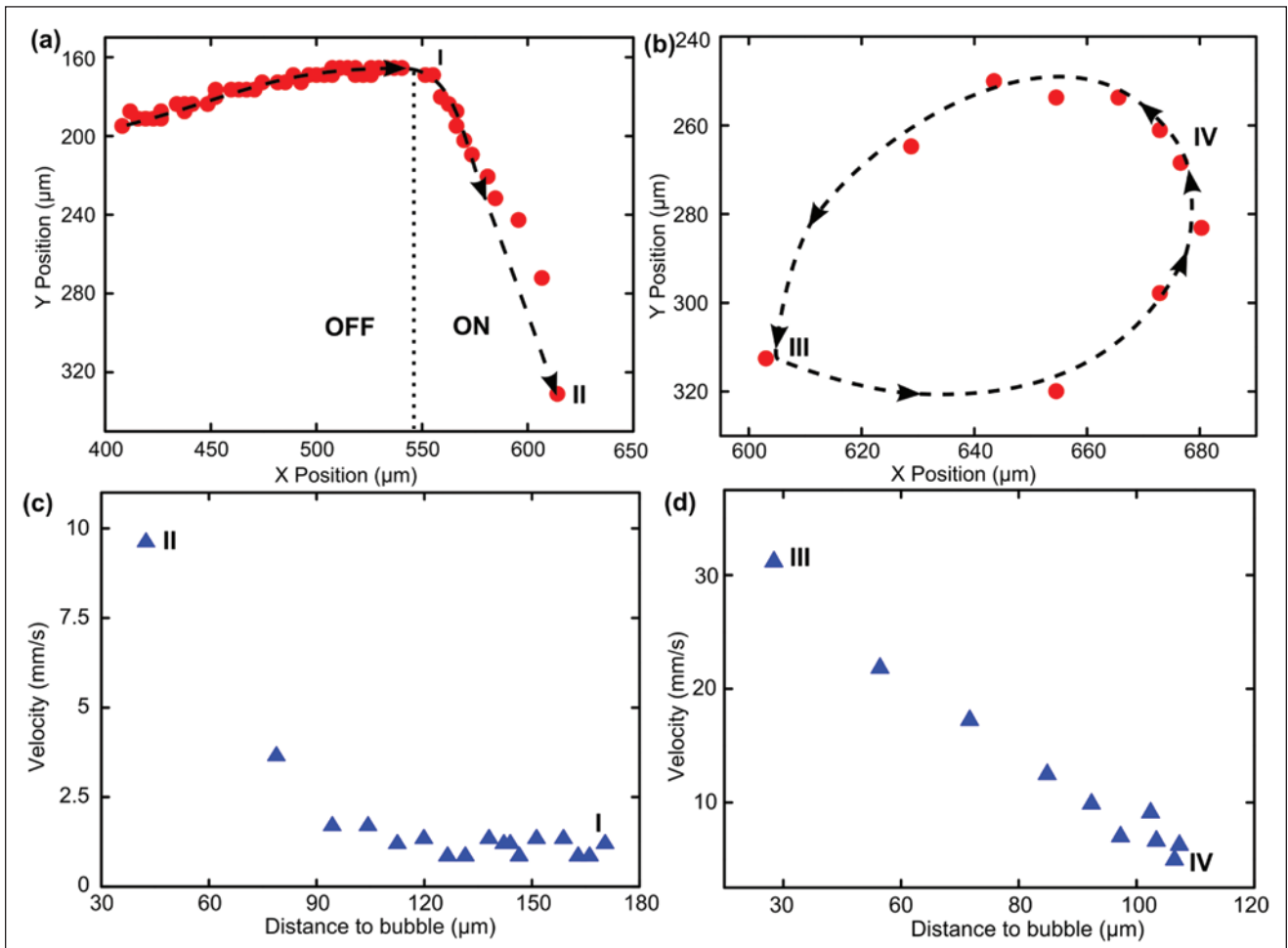


Figure 4. (a, b) Quantitative description of the trajectory of a particle during the attraction process and rotation process, respectively. (c, d) Velocity of a particle during the attraction process and rotation process, respectively.

Fig. 4b), the drag force far surpassed the radiation force (or else the particle would have been trapped on the bubble surface by F_r), and the particle repelled from the bubble at a high speed. At the farthest point in the vortex (point IV in Fig. 4b), the radiation force dominated the drag force, attracting the particle back to the surface of the bubble again. This indicated that the relative velocity between a particle and the surrounding fluid must be small (or else the particle would be removed from the vortex by the flow in the channel). Because of the difficulty in calculating v , eq 6 cannot precisely predict a particle's motion at any given position; however, it provides a qualitative model that will help design and optimize parameters of a working device.

Summary

In summary, we report a bubble-based, acoustofluidic method for trapping and transporting particles in a microfluidic channel. Our approach can precisely position bubbles with prescribed sizes through the use of strategically placed horseshoe-shaped microstructures and thus accurately control the particle-transportation process. By cycling the acoustic waves on and off, the particles were trapped, rotated, and transported among multiple bubbles, causing them to move transversely across the channel via an acoustofluidic relay. We also developed a simple model that balances the effects of drag force and radiation force and provides guiding principles for designing this acoustofluidic device. The technique presented here is useful for the trapping and transport of particles or cells in microfluidic devices and facilitates the further integration of bubble-based, lab-on-a-chip systems.

Acknowledgments

We thank Jason Scott and Nicholas Labarbera for helpful discussion.

Declaration of Conflicting Interests

The authors declared no potential conflicts of interest with respect to the research, authorship, and/or publication of this article.

Funding

The authors disclosed receipt of the following financial support for the research, authorship, and/or publication of this article: This research was supported by National Institutes of Health (Director's New Innovator Award, 1DP2OD007209-01), National Science Foundation, and the Penn State Center for Nanoscale Science (MRSEC). Components of this work were conducted at the Penn State node of the NSF-funded National Nanotechnology Infrastructure Network.

References

- Whitesides, G. M. The Origins and the future of Microfluidics. *Nature* **2006**, *442*, 368–373.

- Neuzil, P.; Giselbrecht, S.; Länge, K.; Huang, T. J.; Manz, A. Revisiting Lab-on-a-Chip Technology for Drug Discovery. *Nat. Rev. Drug. Discov.* **2012**, *11*, 620–632.
- Yang, S.; Guo, F.; Kiraly, B.; Mao, X.; Lu, M.; Huang, T. J. Microfluidic Synthesis of Multifunctional Janus Particles for Biomedical Applications. *Lab Chip* **2012**, *12*, 2097–2102.
- Mao, X.; Huang, T. J. Microfluidic Diagnostics for the Developing World. *Lab Chip*, **2012**, *12*, 1412–1416.
- Sun, Y.; Kim, D. H.; Hashime, A. Biological Cell Sorting Automation. In *Life Science Automation: Fundamentals and Applications*; Zhang, M. J., Nelson, B. J., Felder, R. A., Eds., Artech House Publishers: Norwood, MA, **2007**; pp 411–434.
- Taylor, J.; Ren, C. L.; Stubbley, G. D. Numerical and Experimental Evaluation of Microfluidic Sorting Devices. *Biotechnol. Progr.* **2008**, *24*, 981–991.
- Geislinger, T. M.; Eggart, B.; Braummüller, S.; Schmid, L.; Franke, T. Separation of Blood Cells Using Hydrodynamic Lift. *Appl. Phys. Lett.* **2012**, *100*, 183701–183704.
- Chen, J.; Li, J.; Sun, Y. Microfluidic Approaches for Cancer Cell Detection, Characterization, and Separation. *Lab Chip* **2012**, *12*, 1753–1767.
- Kirby, B. *Micro- and Nanoscale Fluid Mechanics: Transport in Microfluidic Devices*. Cambridge University Press: Cambridge, UK, 2010.
- Zhu, G. P.; Nguyen, N. T. Particle Sorting in Microfluidic Systems. *Micro and Nanosystems* **2010**, *2*, 202–216.
- Lee, G. B.; Chang, C. C.; Huang, S. B.; Yang, R. J. The Hydrodynamic Focusing Effect inside Rectangular Microchannels. *J. Micromech. Microeng.* **2006**, *16*, 1024–1032.
- Davison, S. M.; Sharp, K. V.; Transient Simulations of the Electrophoretic Motion of Cylindrical Particles through a 90 Degree Corner. *Microfluid. Nanofluid.* **2008**, *4*, 409–418.
- Carlo, D. D. Inertial Microfluidics. *Lab Chip* **2009**, *9*, 3038–3046.
- Fu, J.; Mao, P.; Han, J. Continuous-Flow Bioseparation Using Microfabricated Anisotropic Nanofluidic Sieving Structures. *Nat. Protoc.* **2009**, *4*, 1681–1698.
- Mao, X.; Waldeisen, J. R.; Huang, T. J. Microfluidic Drifting: Implementing Three-Dimensional Hydrodynamic Focusing with a Single-Layer Planar Microfluidic Device. *Lab Chip* **2007**, *7*, 1260–1262.
- Mao, X.; Lin, S. C. S.; Dong, C.; Huang, T. J. Single-Layer Planar On-Chip Flow Cytometer Using Microfluidic Drifting Based Three-Dimensional (3D) Hydrodynamic Focusing. *Lab Chip* **2009**, *9*, 1583–1589.
- Cho, S. K.; Zhao, Y.; Kim, C. J. Concentration and Binary Separation of Micro Particles for Droplet-Based Digital Microfluidics. *Lab Chip* **2007**, *7*, 490–498.
- Sin, M. L. Y.; Shimabukuro, Y.; Wong, P. K. Hybrid Electrokinetics for Separation, Mixing, and Concentration of Colloidal Particles. *Nanotechnology* **2009**, *20*, 165701–165709.
- Guo, F.; Ji, X.; Liu, K.; He, R.; Zhao, L.; Guo, Z.; Liu, W.; Guo, S.; Zhao, X. Droplet Electric Separator Microfluidic Device for Cell Sorting. *Appl. Phys. Lett.* **2010**, *96*, 193701–193703.
- Digabel, J.; Biais, N.; Fresnais, J.; Berret, J.; Hersena, P.; Ladoux, B. Magnetic Micropillars as a Tool to Govern Substrate Deformations. *Lab Chip* **2011**, *11*, 2630–2636.

21. Zhu, J.; Liang, L.; Xuan, X. On-Chip Manipulation of Nonmagnetic Particles in Paramagnetic Solutions Using Embedded Permanent Magnets. *Microfluid. Nanofluid.* **2012**, *12*, 65–73.
22. Grier, D. G. A Revolution in Optical Manipulation. *Nature* **2003**, *424*, 810–816.
23. Ohta, A. T. Optically Controlled Cell Discrimination and Trapping Using Optoelectronic Tweezers. *IEEE Journal of Selected Topics in Quantum Electronics* **2007**, *13*, 235–243.
24. Pierce, A. D. *Acoustics: An Introduction to Its Physical Principles and Applications*. Acoustical Society of America: New York; 1989.
25. Shi, J.; Ahmed, D.; Mao, X.; Lin, S. S.; Huang, T. J. Acoustic Tweezers: Patterning Cells and Microparticles Using Standing Surface Acoustic Waves (SSAW). *Lab Chip* **2009**, *9*, 2890–2895.
26. Ding, X.; Lin, S. C. S.; Kiraly, B.; Yue, H.; Li, S.; Chiang, I. K.; Shi, J.; Benkovic, S. J.; Huang, T. J. On-Chip Manipulation of Single Microparticles, Cells, and Organisms Using Surface Acoustic Waves. *Proc. Nat. Acad. Sci. U. S. A.* **2012**, *109*, 11105–11109.
27. Shi, J.; Mao, X.; Ahmed, D.; Colletti, A.; Huang, T. J. Focusing Microparticles in a Microfluidic Channel with Standing Surface Acoustic Waves (SSAW). *Lab Chip* **2008**, *8*, 221–223.
28. Shi, J.; Huang, H.; Stratton, Z.; Huang, Y.; Huang, T. J. Continuous Particle Separation in a Microfluidic Channel via Standing Surface Acoustic Waves (SSAW) *Lab Chip* **2009**, *9*, 3354–3359.
29. Shi, J.; Yazdi, S.; Lin, S. C. S.; Ding, X.; Chiang, I.; Sharp, K.; Huang, T. J. Three-Dimensional Continuous Particle Focusing in a Microfluidic Channel via Standing Surface Acoustic Waves (SSAW) *Lab Chip* **2011**, *11*, 2319–2324.
30. Lin, S. C. S.; Mao, X.; Huang, T. J. Surface Acoustic Wave (SAW) Acoustophoresis: Now and Beyond. *Lab Chip* **2012**, *12*, 2766–2770.
31. Ding, X.; Lin, S. C. S.; Lapsley, M. I.; Li, S.; Guo, X.; Chan, C. Y. K.; Chiang, I.; McCoy, J. P.; Huang, T. J. Standing Surface Acoustic Wave (SSAW) Based Multichannel Cell Sorting. *Lab Chip* **2012**, *12*, 4228–4231.
32. Ding, X.; Shi, J.; Lin, S. C. S.; Yazdi, S.; Kiraly, B.; Huang, T. J. Tunable Patterning of Microparticles and Cells Using Standing Surface Acoustic Waves. *Lab Chip* **2012**, *12*, 2491–2497.
33. Marmottant, P.; Hilgenfeldt, S. Controlled Vesicle Deformation and Lysis by Single Oscillating Bubbles. *Nature* **2003**, *423*, 153–156.
34. Marmottant, P.; Hilgenfeldt, S. A Bubble-Driven Microfluidic Transport Element for Bioengineering. *Proc. Nat. Acad. Sci. U. S. A.* **2004**, *101*, 9523–9527.
35. Ahmed, D.; Mao, X.; Juluri, B. K.; Huang, T. J. A Fast Microfluidic Mixer Based on Acoustically Driven Sidewall-Trapped Microbubbles. *Microfluid. Nanofluid.* **2009**, *7*, 727–731.
36. Wang, S. S.; Jiao, Z. J.; Huang, X. Y.; Yang, C.; Nguyen, N. T. Acoustically Induced Bubbles in a Microfluidic Channel for Mixing Enhancement. *Microfluid. Nanofluid.* **2009**, *6*, 847–852.
37. Rogers, P.; Neild, A. Selective Particle Trapping Using an Oscillating Microbubble. *Lab Chip* **2011**, *11*, 3710–3715.
38. Wang, C.; Jalikop, S. V.; Hilgenfeldt, S. Size-Sensitive Sorting of Microparticles Through Control of Flow Geometry. *Appl. Phys. Lett.* **2011**, *99*, 03410–03413.
39. Xie, Y.; Ahmed, D.; Lapsley, M. I.; Lin, S. C. S.; Nawaz, A. A.; Wang, L.; Huang, T. J. Single-Shot Characterization of Enzymatic Reaction Constants K_m and k_{cat} by an Acoustic-Driven, Bubble-Based Fast Micromixer. *Anal. Chem.*, **2012**, *84*, 7495–7501.
40. Patel, M. V.; Tovar, A. R.; Lee, A. P. Lateral Cavity Acoustic Transducer as an On-Chip Cell/Particle Microfluidic Switch. *Lab Chip* **2012**, *12*, 139–145.
41. Wang, C.; Jalikop, S. V.; Hilgenfeldt, S. Efficient Manipulation of Microparticles in Bubble Streaming Flows. *Biomicrofluidics* **2012**, *6*, 012801–012801-11.
42. Wang, S. S.; Huang, X. Y.; Yang, C. Mixing Enhancement in a Microfluidic Chamber for High Viscous Fluids. *Lab Chip* **2011**, *11*, 845–850.
43. Hashmi, A.; Yu, G.; Reilly-Collette, M.; Heiman, G.; Xu, J. Oscillating Bubbles: A Versatile Tool for Lab on a Chip Applications. *Lab Chip* **2012**, *12*, 4216–4227.
44. Chung, S. K.; Cho, S. K. On-Chip Manipulation of Objects Using Mobile Oscillating Bubbles. *J. Micromech. Microeng.* **2008**, *18*, 125024.
45. Chung, S. K.; Cho, S. K. 3-D Manipulation of Millimeter- and Micro Sized Objects Using an Acoustically-Excited Oscillating Bubble. *Microfluid. Nanofluid.* **2009**, *6*, 261–265.
46. Ryu, K.; Chung, S. K.; Cho, S. K. *Separation and Collection of Microparticles Using Oscillating Bubbles*. The 12th International Conference on Miniaturized Systems for Chemistry and Life Sciences (μ TAS 2008), October 12–16, 2008; San Diego, CA; pp 1471–1473.
47. Ahmed, D.; Chan, C. Y.; Lin, S. C. S.; Muddana, H. S.; Nama, N.; Huang, T. J.; Tunable, Pulsatile Chemical Gradient Generation via Acoustically Driven Oscillating Bubbles. *Lab Chip* **2013**, *13*, 328–331.
48. Ahmed, D.; Mao, X.; Shi, J.; Juluri, B. K.; Huang, T. J. A Millisecond Micromixer via Single-Bubble-Based Acoustic Streaming. *Lab Chip* **2009**, *9*, 2738–2741.
49. Xia, Y.; Whitesides, G. M. Soft Lithography. *Angew. Chem. Int. Ed.* **1998**, *37*, 550–575.
50. Mao, X.; Juluri, B. K.; Lapsley, M. I.; Stratton, Z. S.; Huang, T. J. Milliseconds Microfluidic Chaotic Bubble Mixer. *Microfluid. Nanofluid.* **2010**, *8*, 139–144.
51. Thi, P.; Manasseh, R.; Ool, A. Cavitation Microstreaming Patterns in Single and Multiple Bubble Systems. *J. Fluid. Mech.* **2007**, *576*, 191–233.
52. Leighton, T. G. *The Acoustic Bubble*. London: Academic Press, 1994.
53. Miller, D. L. Particle Gathering and Microstreaming Near Ultrasonically Activated Gas-Filled Micropores. *J. Acoust. Soc. Am.* **1988**, *84*, 1378–1387.
54. Yosioka, K.; Kawasima, Y. Acoustic Radiation Pressure on a Compressible Sphere. *Acustica.* **1955**, *5*, 167–173.